Journal of Power Sources 264 (2014) 229–234

Contents lists available at ScienceDirect

Journal of Power Sources

journal homepage: www.elsevier.com/locate/jpowsour

Hydrothermal synthesis of MoS_2 nanoflowers as highly efficient hydrogen evolution reaction catalysts

Dezhi Wang [a,b], Zhou Pan [a], Zhuangzhi Wu [a,b,c,*], Zhiping Wang [a], Zhihong Liu [c]

[a] School of Materials Science and Engineering, Central South University, Yuelu Road, Changsha, Hunan 410083, PR China
[b] Key Laboratory of Ministry of Education for Non-ferrous Materials Science and Engineering, Central South University, Yuelu Road, Changsha, Hunan 410083, PR China
[c] School of Metallurgical Science and Engineering, Central South University, Changsha 410083, China

HIGHLIGHTS

- Amorphous MoS_2 nanoflowers have been successfully prepared by a hydrothermal method.
- Amorphous MoS_2 nanoflowers exhibit excellent activity and stability in the HER.
- A relatively low Tafel slope of 52 mV dec^{-1} was obtained.
- A small onset potential of −130 mV was also observed.

GRAPHICAL ABSTRACT

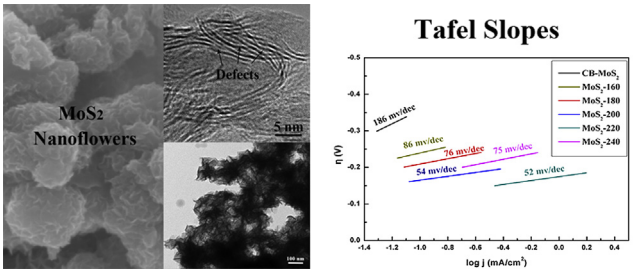

ARTICLE INFO

Article history:
Received 18 December 2013
Received in revised form
9 April 2014
Accepted 14 April 2014
Available online 24 April 2014

Keywords:
Molybdenum disulfide
Hydrogen evolution reaction
Electrocatalyst
Nanoflowers

ABSTRACT

Amorphous MoS_2 nanoflowers assembled by lamellar nanosheets have been successfully synthesized by a facile hydrothermal method. They were characterized by X-ray diffraction (XRD), Raman spectroscopy, scanning electron microscopy (SEM) and transmission electron microscopy (TEM), and evaluated as electrochemical catalysts in the hydrogen evolution reaction (HER). Moreover, the effect of preparation temperature was also discussed. It was found that these catalysts exhibited excellent HER activity compared to commercial bulk MoS_2 microparticles due to the special structure of nanoflowers assembled by nanosheets with few layers, exposing much more active sites and reducing intrinsic resistance. And the catalyst obtained at 220 °C showed the best activity with the largest exchange current density and the smallest Tafel slope of 52 mV dec^{-1}, which made it a promising HER electrocatalyst for practical applications.

1. Introduction

As we all know, hydrogen energy is an ideal, clean and efficient secondary energy resource. It serves as one of the most promising candidates for replacing petroleum fuels in future. The commonest way to obtain hydrogen is water electrolysis, as it is abundant and contains no carbon. Although some noble metals such as Platinum and Palladium are well-known for their superior electrocatalytic property in the HER in an acidic medium and commonly used as electrocatalysts in the applications [1,2], large-scale application of them is limited due to their high prices and global low availabilities [3–6]. To find an inexpensive, highly active, acid-stable HER electrocatalyst has become an urgent need [7–9].

Transitional metal sulfides such as nanometer-scaled MoS_2 and WS_2 have attracted considerable attention recently as inorganic electrocatalysts for HER because of their low cost, high chemical stability and excellent electrocatalytic properties [10,11]. Bulk MoS_2

* Corresponding author. School of Materials Science and Engineering, Central South University, Yuelu Road, Changsha, Hunan 410083, PR China. Tel.: +86 731 88877221.
E-mail address: zwu2012@csu.edu.cn (Z. Wu).

http://dx.doi.org/10.1016/j.jpowsour.2014.04.066
0378-7753/

is a poor catalyst [12], however, nano-crystals of MoS_2 and related metal sulphides are more active [13–15]. Therefore, great efforts have been made to design the composites and structures of MoS_2 so that excellent HER activity can be obtained. Generally, to gain highly active MoS_2 catalysts, there are three strategies: (1) increasing the intrinsic activity of active sites, (2) improving the electrical contact to these sites, and (3) increasing the number of active sites. Ni, Co and Fe were adopted to improve the intrinsic activity [16], and more highly conductive materials were added to improve the electrical contact, including reduced grapheme oxide [17], carbon nanotubes [18], carbon nanospheres [15], and so on. With respect to the last issue, the structure design of MoS_2 has attracted great attentions to obtain more active sites. Kibsgaard engineered the surface structure of MoS_2 to gain preferentially exposed active edge sites adopting a double-gyroid template, presenting a small Tafel slope [19]. Kong proposed a novel chemical vapor deposition method to synthesize MoS_2 films with vertically aligned layers, which show rich active edge sites and possess a Tafel slope of 105–120 mV dec^{-1} [20]. In our previous work, we designed MoS_2 nanosheets with a high active site density by a microdomain method, and a high edge/basal ratio was obtained showing a small Tafel slope of 68 mV dec^{-1} [21]. However, although the active edge planes are highly exposed, the HER activity is still limited due to the high resistance between two adjacent van der Waals bonded S–Mo–S layers. Yu et al. also demonstrated that the catalytic activity of MoS_2 for the hydrogen evolution reaction decreased by a factor of about 4.47 for the addition of every one more layer [22]. Therefore, the design of highly efficient MoS_2 catalyst for the HER not only desires more active edge sites associated with higher stacking, but also requires lower intrinsic resistance associated with lower stacking. Remarkably, there is a contradiction between the intrinsic resistance and active sites related to the stacking height, and a suitable balance must be approached for the design of a highly active MoS_2 HER catalyst.

In the present work, a novel structure of MoS_2 nanoflower assembled by nanosheets with few layers has been synthesized via a simple hydrothermal method using Na_2S as the sulfide agent. Due to the highly exposed edge sites and relatively low stacking height, a suitable balance and excellent HER activity can be expected, and the effect of preparation temperature was also discussed.

2. Experimental

2.1. Preparation of amorphous MoS_2

A typical procedure is shown as follows. 0.88 g Ammonium molybdate ($(NH_4)_6Mo_7O_{24}\cdot 4H_2O$) was dissolved in 10 ml of distilled water, and then 8 ml of hydrazine monohydrate ($N_2H_4\cdot H_2O$, 86%) as reducing agent was injected. The mixture solution was stirred for 0.5 h, and then 2.64 g $Na_2S\cdot 9H_2O$ dissolved in 10 ml of distilled water and 10 ml of hydrochloric acid was injected and stirred for another 10 min. The final solution was transferred into a 100 ml Teflon-lined stainless steel autoclave and heated at 160 °C for 12 h. After filtering, black powders were collected, dried at 60 °C for 5 h and then retained for use. Other samples were also prepared in the same way with different preparation temperatures at 180 °C, 200 °C, 220 °C and 240 °C, respectively. And the samples were marked as MoS_2-160, MoS_2-180, MoS_2-200, MoS_2-220 and MoS_2-240 associated with their preparation temperatures. Commercial bulk MoS_2 microparticles were also selected to give a comparison, marked as CB-MoS_2.

2.2. Physical characterization

X-ray powder diffraction (XRD) patterns for the various electrocatalysts were recorded using a D/max-2500 system with Cu Kα radiation ($\lambda = 0.154$ nm). Raman spectroscopy was recorded using the instrument LabRAMHR-800 of French company HRIBA. Microstructures were observed by the scanning electron microscopy (SEM, FEI Sirion 200) and transmission electron microscopy (TEM, JEOL-2010).

2.3. Electrochemical characterization

Typically, 1 mg of amorphous MoS_2 catalyst and 80 μL Nafion solution (5 wt%) were dispersed in 1 ml of a solution composed of 200 μL ethanol and 800 μL distilled water. After sonication for 30 min, 5 μL of the catalyst slurry was dropped onto the surface of a GCE (glassy carbon electrode) (3 mm in diameter). And then the GCE was dried at room temperature to yield a catalyst loading of 71 μg cm^{-2}.

The electrochemical measurements were carried out in a standard three-electrode setup. The electrocatalytic activity of MoS_2 was examined through linear sweep voltammetry (LSV) with a scan rate of 2 mV s^{-1} on an IM6ex (Zahner, Germany) in 0.5 M H_2SO_4 at room temperature. A saturated calomel electrode (SCE) was employed as the reference electrode and a Pt foil as the counter electrode. Electrode potentials were recorded vs SCE reference electrode, which was calibrated with respect to reversible hydrogen electrode (RHE). Before the electrochemical measurements, the electrolyte solution was purged with N_2 for 1 h to remove completely the oxygen, and stable polarization curves were recorded after 20 cycles. The turnover frequencies were calculated from the exchange current densities using the following relation [12]:

$$\mathrm{TOF}\,(s^{-1}) = (j_0, \mathrm{A\,cm^{-2}})/[(1.5\times 10^{15}\ \mathrm{sites\,cm^{-2}})\,(1.602\times 10^{-19}\ \mathrm{C/e^-})\,(2e^-/H_2)]$$

3. Results and discussion

3.1. Structure characterization

X-ray powder diffraction (XRD) patterns of various samples obtained at different temperatures are shown in Fig. 1. We can see that all the XRD patterns present low diffraction peaks of (002) compared to bulk CB-MoS_2 (inset), indicating poor crystallinity. However, the slight (100) and (110) diffraction peaks still can demonstrate the existence of MoS_2 [23]. With the increased

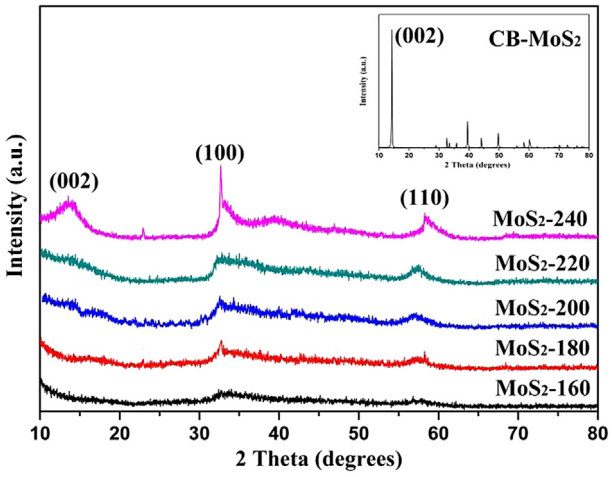

Fig. 1. XRD patterns of the catalysts obtained at various temperatures and CB-MoS_2 (inset).

temperature, the intensity of diffraction peaks becomes sharper, indicating the improvement of crystallinity. Especially, the location of (110) peak also shifted to the high angles with the increased temperature. More importantly, the absence of the (002) diffraction peak indicates a low stacking height along this direction. And the (002) only becomes remarkable at 240 °C, demonstrating a higher stacking height along the *c*-axis. It is noteworthy that all the peaks are significantly broadened than the pristine 2H-MoS_2 (JCPDS Card No.73-1508) due to the worse crystallinity and smaller particle size. High HER activity can be expected because of the absence of (002) peaks leading to lower intrinsic resistance at low temperatures (160–220 °C).

Raman spectroscopy was employed to further confirm the MoS_2 phase, where the appearance of two peaks at 287 and 380 cm^{-1} corresponds to the E_{1g} and E^1_{2g} vibrational models of hexagonal MoS_2, respectively (Fig. 2). It is known that the E_{1g} and E^1_{2g} correlate with the relative vibration mode along the layer of the bond between Mo and S. And the E^1_{2g} peak presents the in-layer displacements of Mo and S atoms [24,25]. The relatively larger E^1_{2g} peak width and the weaker intensity suggest that the crystal structure of MoS_2 may contain substantial defect sites [26]. Moreover, a mode around 460 cm^{-1} arises from a second-order process involving the longitudinal acoustic phonons at M point (LA(M)) at a high temperature of 240 °C [27]. With the increased temperature, the peaks E_{1g} and E^1_{2g} become higher and sharper, demonstrating a reduction of defects and better crystallinity. However, it must be noted that the Raman peak corresponding to the out-of plane Mo–S phonon mode (A_{1g}, 408 cm^{-1}) is absent, indicating that the relative vibration along the direction of vertical layer of the bond between Mo and S is not significant, which is also coincident with the absence of (002) peak in Fig. 1.

Due to the similarity of catalysts obtained at low temperatures (160–220 °C), only the MoS_2-220 catalyst is selected to represent the typical morphologies and structures, as shown in Fig. 3. The SEM images provide a general view, and show that the catalysts are nanoflowers with a diameter of 100–500 nm, assembled by lamellar nanosheets (Fig. 3a and b). However, indicated by the XRD pattern, the size of MoS_2-240 is much larger with remarkable aggregations, as shown in Fig. S1 (Supporting information). A further insight was obtained by TEM. It can be observed that these nanoflowers are assembled by nanosheets, which are about 100 nm in length and 10 nm in thickness, respectively, as shown in Fig. 3c. More information is obtained in Fig. 3d with a higher magnification. It can be observed that the MoS_2 nanosheets are short with low stacking height, presenting an expanded interlayer distance of 0.8 nm, much larger than the standard value of 0.62 nm, indicating a significant lattice expansion [13]. More importantly, there are

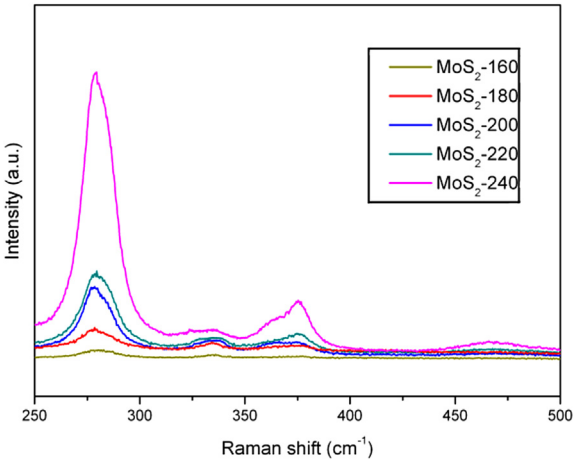

Fig. 2. Raman spectra of various MoS_2 samples.

many defects in the stacking structures, as shown in the insert image of Fig. 3d, which increase the interlayer resistance and will lead to a remarkable decrease of the final HER activity. Although the previous XRD and Raman analysis demonstrate the absence of (002) peaks and layer stacking along *c*-axis, there are still stacking structures observed with expanded interlayers. This abnormal phenomenon should be attributed to the existence of rich defects, which greatly deteriorate the crystallinity, leading to the missing of related XRD and Raman signals.

3.2. Electrocatalytic activity toward the HER

The polarization curves of all the samples measured in 0.5 M H_2SO_4 with a scan rate of 2 mV s^{-1} at room temperature are shown in Fig. 4. All the MoS_2 samples exhibit much better activity than the commercial bulk MoS_2 (−350 mV) with more positive onset potentials between −130 and −220 mV, which can be attributed to the special nanoflower structures assembled by nanosheets. Generally, it is widely accepted that the HER active sites are located on the edge planes [12,21]. And tailoring the microstructures of MoS_2 to obtain more exposed edge planes can greatly enhance the HER activity. In the present case, compared to the commercial microparticles, the MoS_2 nanoflowers assembled by lamellar nanosheets possess much more exposed edge planes, which can significantly improve the final HER activity. Among these catalysts, the MoS_2-220 shows the best HER activity with the most positive onset potential of −130 mV and a current density of 13.8 mA cm^{-2} at −300 mV, which is nearly 77 times larger than that of the CB-MoS_2 (0.18 mA cm^{-2}). However, each amorphous MoS_2 sample exhibits a quite different catalytic activity, which is decided by their intrinsic structures. As shown in Fig. 4, with the increased preparation temperature, the HER activity of MoS_2 samples firstly is increased and reaches the maximum value at 220 °C, then drops down sharply afterward. MoS_2-160 shows the worst catalytic activity among these amorphous MoS_2 catalysts with an onset potential of −220 mV and a current density of 0.432 mA cm^{-2} at −300 mV, but still better than CB-MoS_2. The catalysts obtained at low temperatures generally contain rich defects, which can provide more active sites and is beneficial to the final HER activity. However, more defects also make in-layer conductivity worse at the same time. Therefore, there is a balance between more active sites and worse conductivity. With the increased temperature, the crystallinity is improved, indicating less defects and better conductivity. And the latter plays the predominant role in the final HER activity. Therefore, the activity is enhanced gradually with the increased temperatures from 160 to 220 °C, and reaches the maximum value at 220 °C. However, a higher temperature (240 °C) promoted the significant improvement of crystallinity, resulting in a remarkable (002) diffraction peak, indicating a higher stacking, as shown in Fig. 1. It must be noted that the resistance between layers of MoS_2 is much larger than that in layers, which will greatly deteriorate the HER activity [28,29]. As a result, the activity of MoS_2-240 is even worse than that of MoS_2-200 due to less defects and worse conductivity.

A smaller Tafel slope means a faster increase of the HER rate with increased potentials. The Tafel plots of these amorphous MoS_2 samples derived from the polarization curves shown in Fig. 4 fit well with the Tafel equation ($\eta = b\log j + a$, where j is the current density and b is the Tafel slope) at different overpotential ranges, as shown in Fig. 5. The Tafel slope of these amorphous MoS_2 samples are between 52 and 86 mV dec^{-1}, much smaller than that of the CB-MoS_2 (186 mV dec^{-1}). Moreover, the MoS_2-220 shows the minimum value of 52 mV dec^{-1}, which is consistent with the most positive onset potential of −130 mV. The smaller Tafel slope demonstrates that the amorphous MoS_2 catalysts possess a superior catalytic performance. Herein, the as-obtained Tafel slope of

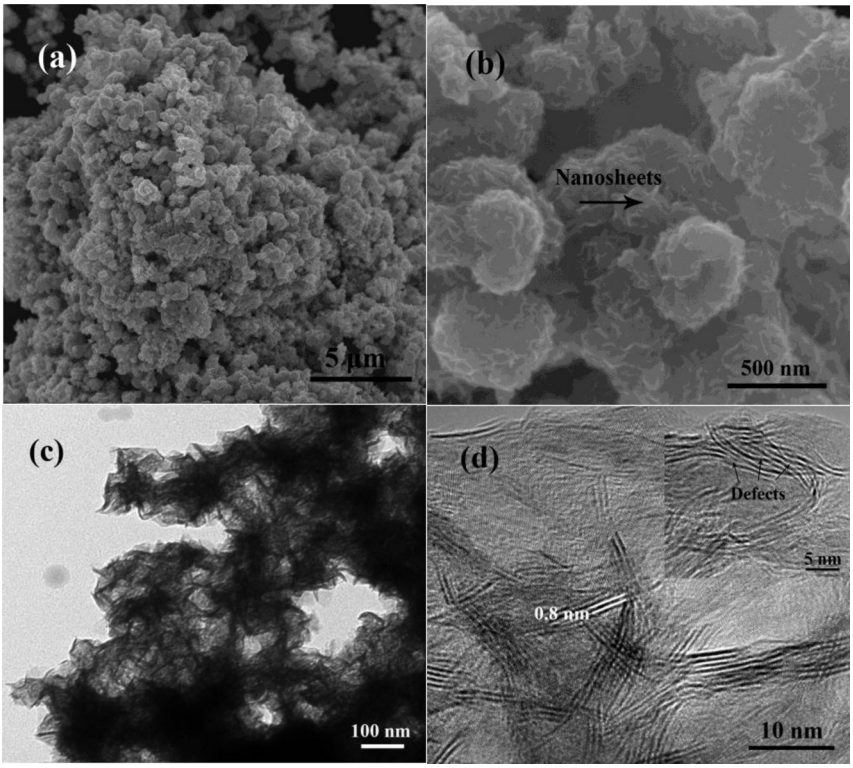

Fig. 3. SEM (a and b) and TEM (c and d) images of MoS_2-220.

52 mV dec^{-1} for MoS_2-220 is among the lowest records for single component MoS_2 electrocatalysts for the HER [19,30,31]. Three possible reaction steps have been proposed for the HER in acidic solutions [32–34]:

Discharge reaction (Volmer):

$$H_3O^+ + e^- \rightarrow H_{ads} + H_2O \quad (1)$$

Electrochemical desorption reaction (Heyrovsky):

$$H_{ads} + H^+ + e^- \rightarrow H_2 \quad (2)$$

Combination reaction (Tafel):

$$H_{ads} + H_{ads} \rightarrow H_2 \quad (3)$$

Generally, a fast discharge reaction (1) followed by a rate-limiting combination reaction (3) leads to a Tafel slope of 30 mV dec^{-1}. When (1) is fast and followed by a slow electrochemical desorption (2), a Tafel slope of 40 mV dec^{-1} is obtained. Moreover, if (1) is rate-limiting, the Tafel slope is 120 mV dec^{-1}. While these values can be adopted as a guide in identifying the HER mechanisms, it must be noted that these calculations are based on a strict set of assumptions that do not universally hold. Thus,

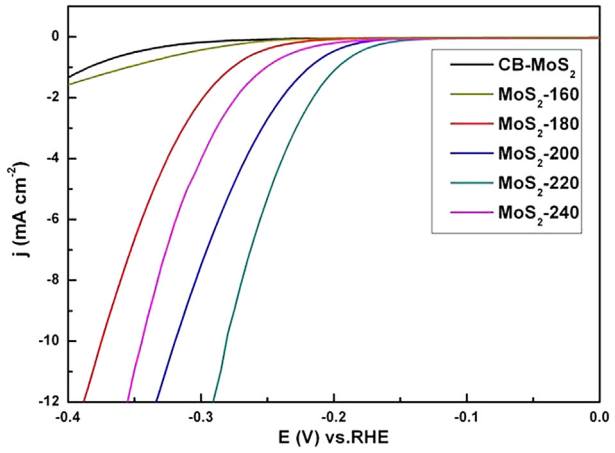

Fig. 4. The polarization curves of all the catalysts.

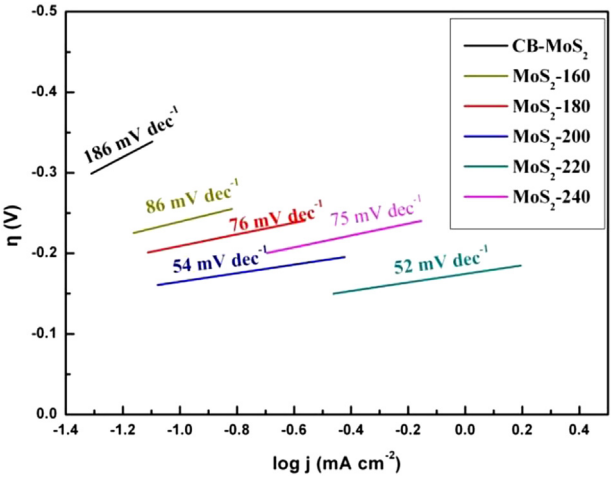

Fig. 5. The Tafel plots of the MoS_2 catalysts derived from the polarization curves.

Table 1
Tafel slopes, onset potentials, exchange current densities j_0, and turnover frequencies (TOFs) for various MoS_2 catalysts.

Catalyst	Tafel slope (mV dec^{-1})	Onset potential (mV)	j_0 ($\times 10^{-6}$ A cm^{-2})	TOF (s^{-1})
CB-MoS_2	186	−350	0.34	0.007
MoS_2-160	86	−220	5.94	0.012
MoS_2-180	76	−165	7.08	0.015
MoS_2-200	54	−150	8.24	0.017
MoS_2-220	52	−130	14.59	0.03
MoS_2-240	75	−200	7.59	0.016

identifying the HER mechanism according to the Tafel slope analysis alone is not always clear [32–34]. And herein, it only can be concluded that the mechanism is a fast discharge reaction (1) followed by either a rate-limiting Heyrovsky reaction or Tafel reaction. As a result, these two possible mechanisms cannot be distinguished completely at all. However, the Tafel slope of 52 mV dec^{-1} in the current work closely matches the engineered MoS_2 nanoparticles with highly exposed active edge sites, suggesting a similarity in surface chemistry for these two catalysts despite differences in morphology and preparation method [34].

The most inherent measure of activity for the HER is the exchange current density, j_0, which is determined by fitting j-E data to the Tafel equation [12]. The exchange current density values of all the samples are listed in Table 1. We can see that j_0 values of all the amorphous MoS_2 samples are larger than that of CB-MoS_2. The most active catalyst of MoS_2-220 shows the largest exchange current density of 14.59 μA cm^{-2}, which is about 43 times larger than that of CB-MoS_2 (0.34 μA cm^{-2}).

To get a direct site-to-site comparison, the rough estimation of TOFs following Jaramillo's method [12], as shown in Table 1, makes it possible to compare the activity of amorphous MoS_2 with other catalysts. The so-called TOF here was actually defined as the per-atom exchange rate of Mo, where the active sites were probably located. Compared to CB-MoS_2, the amorphous MoS_2 catalysts possess much higher values of TOF, and especially the MoS_2-220 shows the highest TOF value of 0.03 s^{-1}, which is even superior to the MoS_2 nanoparticles deposited on Au by UHV [12], indicating an excellent intrinsic HER activity.

Besides the HER activity, the stability is another important criterion to evaluate the HER electrocatalyst. To study the stability in acidic environment, long-term potential cycling stability of MoS_2-220 was conducted by taking a potential scan from −0.4 to 0.1 V for 1000 cycles with an accelerated scanning rate of 100 mV s^{-1}. It can be seen that there is only a slight activity loss after 1000 cycles, as shown in Fig. 6, indicating a good durability, consistent with the previous reported MoS_2-based electrocatalysts [34,35].

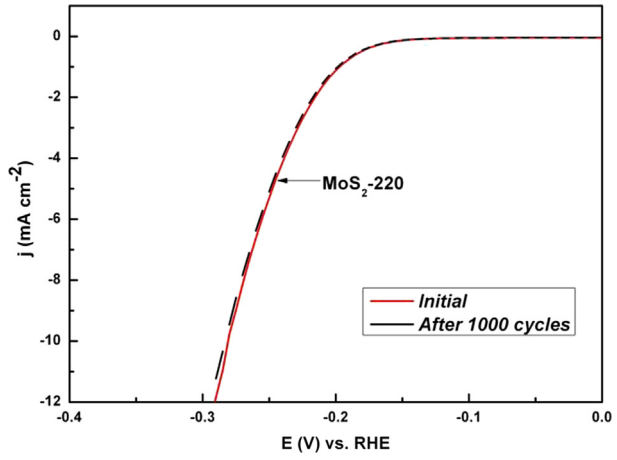

Fig. 6. Durability test of MoS_2-220 showing negligible loss after 1000 cycles.

4. Conclusion

In summary, amorphous MoS_2 nanoflowers assembled by nanosheets with few layers have been successfully prepared and present excellent HER activity due to their highly exposed active sites and relatively low intrinsic resistance. The catalyst MoS_2-220 exhibits the best HER activity with the smallest Tafel slope of 52 mV dec^{-1}, the most positive onset overpotential of −130 mV and the highest TOF of 0.03 s^{-1}, making it a promising HER electrocatalyst for practical applications. Rich defects obtained at low temperatures not only provide more active sites but also deteriorate the conductivity at the same time, and an optimized balance is obtained at 220 °C, resulting in the best HER activity. This work paves a way to synthesize highly active HER catalysts with special designed structures exposing more active sites, and broadens our vision to improve the activity of various electrocatalysts by synergistically structural and electronic modulations.

Acknowledgments

Financial supports from the National Natural Science Foundation of China (Grant No. 51302326) and the Postdoctoral Science Foundation of China (Grant No.2013M531801) are gratefully acknowledged.

Appendix A. Supplementary data

Supplementary data related to this article can be found at http://dx.doi.org/10.1016/j.jpowsour.2014.04.066.

References

[1] F. Raimondi, G.G. Scherer, R. Kotz, A. Wokaun, Angew. Chem. Int. Ed. 44 (2005) 2190–2209.
[2] R. Tolle, A. Otto, Surf. Sci. 597 (2005) 110–118.
[3] M. Arenz, V. Stamenkovic, T.J. Schmidt, K. Wandelt, P.N. Ross, M. Markovic, Surf. Sci. 506 (2002) 287–296.
[4] B. Fang, J. Kim, J.S. Yu, Electrochem. Commun. 10 (2008) 659–662.
[5] Z. Wu, B. Fang, A. Bonakdarpour, A. Sun, D. Wilkinson, Appl. Catal. B Environ. 125 (2012) 59–66.
[6] N.R. Elezovic, L. Gajic-Krstajic, V. Radmilovic, L. Vracar, N.V. Krstajic, Electrochim. Acta 54 (2009) pp.1375–1382.
[7] M.G. Walter, E.L. Warren, J.R. Mckone, S.W. Boettcher, Q.X. Mi, E.A. Santori, N.S. Lewis, Chem. Rev. 110 (2010) 6446–6473.
[8] Y. Li, G.A. Somorjai, Nano. Lett. 10 (2010) 2289–2295.
[9] Y.D. Hou, B.L. Abrams, P.C.K. Vesborg, M.E. Bjorketun, K. Herbst, L. Bech, A.M. Stti, C. Damsgaard, T. Pedersen, O. Hansen, J. Rossmeisl, S. Dahl, J.K. Norskov, I. Chorkendorff, Nat. Mater. 10 (2011) 434–438.
[10] D. Merki, X. Hu, Energy Environ. Sci. 4 (2011) 3878–3888.
[11] H. Vrubel, D. Merki, X. Hu, Energy Environ. Sci. 5 (2012) 6136–6144.
[12] T.F. Jaramillo, K.P. Jorgensen, J. Bonde, J.H. Nielsen, S. Horch, I. Chorkendorff, Science 317 (2007) 100–102.
[13] D. Wang, Z. Wang, C. Wang, P. Zhou, Z. Wu, Z. Liu, Electrochem. Commun. 34 (2013) 219–222.
[14] J.D. Benck, Z. Chen, L.Y. Kuritzky, A.J. Forman, T.F. Jaramillo, ACS. Catal. 2 (2012) 1916–1923.
[15] X. Bian, J. Zhu, L. Liao, M.D. Scanlon, P. Ge, C. Ji, H.H. Girault, B. Liu, Electrochem. Commun. 22 (2012) 128–132.
[16] D. Merki, H. Vrubel, L. Rovelli, S. Fierro, X. Hu, Chem. Sci. 3 (2012) 2515–2525.
[17] Y. Li, H. Wang, L. Xie, Y. Liang, G. Hong, H. Dai, J. Am. Chem. Soc. 133 (2011) 7296–7299.
[18] T. Lin, C. Liu, J. Lin, Appl. Catal. B Environ. 134 (2013) 75–82.
[19] J. Kibsgaard, Z. Chen, B.N. Reinecke, T.F. Jaramillo, Nat. Mater. 11 (2012) 963–969.
[20] D. Kong, H. Wang, J. Cha, M. Pasta, K.J. Koski, J. Yao, Y. Cui, Nano. Lett. 13 (2013) 1341–1347.
[21] Z. Wu, B. Fang, Z. Wang, C. Wang, Z. Liu, F. Liu, W. Wang, A. Alfantazi, D. Wang, D.P. Wilkinson, ACS. Catal. 3 (2013) 2101–2107.
[22] Y. Yu, S. Huang, Y. Li, S.N. Steinmann, W. Wang, L. Cao, Nano. Lett. 14 (2014) 553–558.

[23] Y. Tian, Y. He, Y. Zhu, Mater. Chem. Phys. 87 (2004) 87–90.
[24] C. Lee, H. Yan, L.E. Brus, T.F. Heinz, J. Hone, S. Ryu, ACS Nano. 4 (2010) 2695–2700.
[25] B.C. Windom, W.G. Sawyer, D.W. Hahn, Tribol. Lett. 42 (2011) 301–310.
[26] K. Liu, W. Zhang, Y. Lee, Y. Lin, M. Chang, C. Su, C. Chang, H. Li, Y. Shi, H. Zhang, C. Lai, L. Li, Nano. Lett. 12 (2012) 1538–1544.
[27] H. Li, Q. Zhang, C. Yap, B. Tay, T. Edwin, A. Olivier, D. Baillargeat, Adv. Funct. Mater. 22 (2012) 1385–1390.
[28] A.B. Laursen, S. Kegnas, S. Dahl, I. Chorkendorff, Energy Environ. Sci. 5 (2012) 5577–5591.
[29] Y. Yan, B. Xia, X. Qi, H. Wang, R. Xu, J. Wang, H. Zhang, X. Wang, Chem. Commun. 49 (2013) 4884–4886.
[30] M.A. Lukowski, A.S. Daniel, F. Meng, A. Forticaux, L. Li, S. Jin, J. Am. Chem. Soc. 135 (2013) 10274–10277.
[31] J. Benck, Z. Chen, L. Kuritzky, A. Forman, T.F. Jaramillo, ACS. Catal. 2 (2012) 1916–1923.
[32] B.E. Conway, B.V. Tilak, Electrochim. Acta 47 (2002) 3571–3594.
[33] S. Ji, Z. Yang, C. Zhang, Z. Liu, W. Tjiu, I. Phang, Z. Zhang, J. Pan, T. Liu, Electrochim. Acta 109 (2013) 269–275.
[34] Z. Chen, D. Cummins, B. Reinecke, E. Clark, M. Sunkara, T. Jaramillo, Nano. Lett. 11 (2011) 4168–4175.
[35] T. Wang, L. Liu, Z. Zhu, P. Papakonstantinou, J. Hu, H. Liu, M. Li, Energy Environ. Sci. 6 (2013) 625–633.